CFD investigation of a multi-tube photocatalytic reactor in non-steady-state conditions

CFD investigation of a multi-tube photocatalytic reactor in non-steady-state conditions

Jeroen van Walsem[†], Sammy W. Verbruggen[†], Bart Modde[§], Silvia Lenaerts[†], Siegfried Denys[†,]*

† Sustainable Energy, Air & Water Technology, Department of Bioscience Engineering, University of Antwerp, Groenenborgerlaan 171, B-2020 Antwerp, Belgium.

§ Vento Ltd., Bedrijvenpark Coupure 5, B-9700 Oudenaarde, Belgium.

* E-mail: Siegfried.Denys@uantwerp.be

Fax: +32 3 265 32 25. Tel: +32 3 265 32 30.

Keywords

CFD; multiphysics; adsorption; photocatalysis; acetaldehyde; kinetics

Highlights

- A novel multi-tube photoreactor with high conversion rates is presented
- All photocatalytic related parameters are accurately determined by CFD
- Also non-steady-state adsorption and photocatalytic regimes are accurately modelled
- Adsorption and desorption rate constants change during illumination
- The model is validated by an experiment under challenging transient conditions

Abstract

A novel multi-tube photoreactor is presented with demonstrated high efficiency toward the degradation of acetaldehyde in air. A CFD model is developed to simulate the transient adsorption and photocatalytic degradation processes of acetaldehyde in this reactor design. The CFD model takes into account the entire reactor geometry and all relevant flow parameters, in contrast to analytical methods that often oversimplify the physical and chemical process characteristics. Using CFD, we show that the adsorption and desorption rate constants are not the same under dark and irradiated conditions, which clearly affects the transient behavior. An ultimate validation test in which non-steady adsorption and photocatalytic phenomena occur simultaneously is performed to demonstrate the reliability and accuracy of all parameters obtained from the modelling approach.

1. Introduction

People living in industrial countries spend nearly 90% of their time indoors. Increasingly stringent heat-insulation measures and insufficient ventilation have a negative impact on indoor air quality [1]. Many volatile organic compounds (VOCs) have been identified which may trigger different diseases, commonly referred to as the sick building syndrome [2,3]. The two main strategies to reduce indoor VOC levels are ventilation and air purification. The ventilation strategy suffers from the disadvantages of energy cost and –depending on the circumstances– poor outdoor air quality. Therefore, significant research efforts are directed toward advanced indoor air purification methods. Integration or retrofitting of a photocatalytic (PCO) air purifying unit into heating, ventilation and air conditioning (HVAC) equipment is an interesting approach [4–6]. PCO technology exposes a catalyst, mostly titanium dioxide (TiO_2), to UV light to produce reactive hydroxyl radicals ($OH^{\bullet}$) and superoxide anions ($O_2^{\bullet -}$) that are able to mineralize harmful VOCs into H_2O and CO_2 [7]. PCO technology is cost-effective [8], efficient and ideally it does not produce any waste streams [9].

Designing an efficient PCO reactor for indoor air purification presents specific challenges toward a large number of design parameters. As a general rule, an efficient PCO reactor should have a high degradation efficiency, high photon utilization and low pressure drop and power consumption, in a physically compact vessel [10]. The reactor performance depends partly on the substrate that is used to immobilize the photocatalyst. In one of our previous studies glass fiber mats have been selected as a suitable substrate material [11]. Its open structure offers sufficient light penetration, limited pressure drop, silent operation conditions and a high filtering capacity. A drawback of glass fiber mats is that TiO_2 immobilization and adhesion are difficult, which is primordial for safeguarding human health with nano TiO_2 [12–14].

As a first point of novelty in this work, we present an excellent alternative substrate based on coated glass tubes that are closely packed to constitute a transparent monolith-like architecture. Since the operation of PCO reactors is based on a complex interaction of physical and chemical processes, it is useful to develop mathematical models that include all these phenomena as a tool for reactor design and optimization. By making use of such dynamic models excessive, time-consuming and expensive experimental research can be minimized. These models can also be used to determine the intrinsic kinetic parameters of the photocatalytic system, another crucial step in the development of PCO technology. For instance, we have shown in previous work that computational fluid dynamics (CFD) can accurately deliver the Langmuir Hinshelwood photocatalytic kinetic parameters from steady state experiments in a continuous reactor [15], as well as the Langmuir adsorption/desorption parameters from dynamic, transient experiments [11]. In this work we use CFD modelling to accurately determine pollutant concentrations, adsorption, desorption and kinetic rate constants in a packed glass multi-tube PCO reactor during transient operating regimes. This way not only the adsorption/desorption rate constants and the maximum adsorption capacity of the photocatalyst can be determined, but also the PCO reaction rate constant can be derived from a single mathematical model that

takes into account the complex interplay of all these phenomena for realistic operation conditions. This provides additional insights over existing photocatalytic kinetic studies, that are mostly based on simplified analytical analysis of steady-state situations or batch experiments [16–18]. This study therefore presents a promising strategy for the future design, development and up scaling of PCO air purifying units.

2. Methodology

2.1 Photocatalytic test reactor and coated glass tubes

The photocatalytic test reactor consisted of a borosilicate glass tube with an internal diameter of 22 mm and a length of 440 mm. The reactor was provided with inlet and outlet connections (diameter 4 mm) perpendicular to its longitudinal axis and a closing mechanism using butyl rubbers to seal both ends airtight. A 25 W UV-A lamp (Philips) was positioned above and parallel to the reactor housing at a height of 22 mm, resulting in an incident intensity on the glass tubes of 2.1 mW cm^{-2}, as measured by a calibrated Avantes Avaspec-3648 spectrometer. Three glass tubes with an internal diameter of 7 mm, external diameter of 9 mm and a length of 200 mm were dip-coated using a P25 based powder-modified sol-gel method [19]. For this coating procedure titanium isopropoxide (TTIP, >98%, Acro organics), isopropanol (i-PrOH, >98% VWR chemicals), diethanolamine (DEA, 99% Roth) and Aeroxide P25 (Evonik) were used. A suspension of 3 g P25 in 50 mL isopropanol was made and ultrasonically stirred for 20 min. Thereafter, 8.53 g TTIP and 12.63 g DEA were added while stirring. After 2 h of stirring, 1.08 mL H_2O was added to complete the synthesis. This coating shows improved adhesion properties compared to a standard P25 titanium dioxide suspension but requires a subsequent calcination step at 500°C for 1 h. The adhesion of catalyst particles to the substrate was evaluated by means of the classic Scotch Tape test, as well as by monitoring the amount of released nanoparticles, using designated equipment (P-trak, TSI systems), after placing the coated substrate in a gas flow under 7 bar pressure. The coated substrates showed no particle

loss and could thus be selected for the experiments. The three coated glass tubes were placed in the borosilicate glass tube with their length parallel to the air flow. A schematic overview of the reactor is shown in Figure 1.

2.2 Adsorption/desorption and photocatalytic experiments

Acetaldehyde was used as model compound for indoor air contamination [15,20–23]. In short, acetaldehyde (Praxair, 1% in N_2) was mixed with clean air (Praxair) using mass flow controllers and dosed to the reactor set-up at inlet concentrations that varied between 20 and 220 ppmv in air at a fixed total gas flow rate of 400 cm^3/min. The concentration of acetaldehyde was monitored on-line using FTIR spectroscopy by means of the IR peak height at 2728 cm^{-1}, corresponding to the ν(C-H) stretch vibration. Prior to each experiment the three glass tubes were irradiated by UV light for 12 hours in order to remove any adsorbed organic rest fractions on the TiO_2 surface originating from the coating procedure. During this 'cleaning' phase a total gas flow rate of 400 cm^3/min was applied to stimulate desorption of organics and degradation products.

Adsorption/desorption and photocatalytic reaction experiments were performed in three phases: (1) 420 seconds in by-pass mode during which the gas flow is sent directly to the FTIR detection cell without passing through the reactor, in order to determine the reference concentration level of acetaldehyde, (2) 3600 seconds gas flow through the reactor in dark conditions in order to achieve adsorption-desorption equilibrium, and finally (3) 3600 seconds gas flow through the reactor under illumination during which PCO takes place. These adsorption-desorption and PCO experiments were performed for 3 different concentrations of acetaldehyde and served as input for modelling and parameter estimation purposes. From the transient acetaldehyde bulk concentrations measured by FTIR at the reactor outlet during the second phase of the experiments, adsorption/desorption rate constants were determined for dark conditions. The obtained values served as input parameters for estimating the PCO reaction rate constant from

the transient bulk concentrations during the third phase. By performing the experiments in subsequent phases, the number of parameters to be estimated simultaneously could be limited.

To evaluate the validity of the obtained intrinsic kinetic parameters, an additional experiment was performed in which the gas flow is switched directly from bypass-mode (phase 1) to reactor-illumination mode (phase 3). In this case adsorption/desorption and photocatalytic reaction processes all occur simultaneously in non-steady-state conditions, which makes data modelling quite challenging and thus provides the ultimate test-case for parameter validation.

2.3 Multiphysics Modeling

2.3.1 Air flow modelling and acetaldehyde transport

The commercial software package Comsol Multiphysics v.5.1 was used to perform all theoretical simulations. The complete reactor setup, including the FTIR detection cell, was built in the CFD geometry (Figure 1). Also the thin tubes of 4 mm internal diameter connecting the by-pass switch valve with the test reactor as well as the reactor with the FTIR detection cell were included in the computational geometry since they also contain a small volume of air that should not be neglected. The length of the connecting tubes before and after the test reactor were 1.5 m and 2.5 m, respectively. In order to keep Figure 1 clear, the lengths of the connecting tubes are not shown to scale.

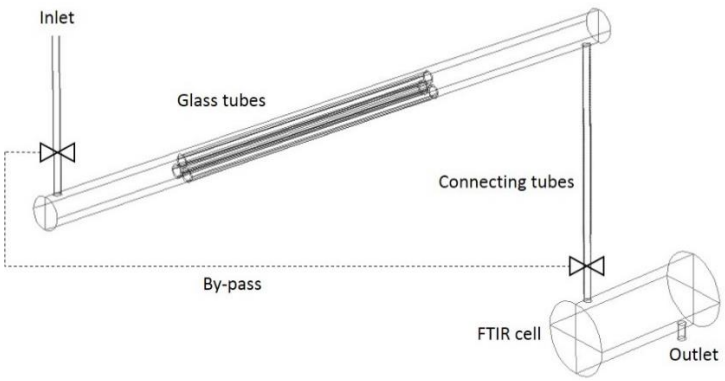

Figure 1: CFD geometry including the test reactor, connecting tubes and FTIR detection cell.

For simplification and to reduce computation time, only half of the geometry was meshed (Figure 2). To ensure mesh quality, a user-defined mesh was created with an average mesh quality of 0.65. Since the main air flow direction is parallel to the length of the connecting tubes and the reactor, it was possible to reduce the number of mesh elements by using prism elements in a substantial part of the geometry. A total of 54,600 prism elements were needed to guarantee a sufficiently fine mesh for these parts. For the inlet and outlet sections of the reactor and the FTIR detection cell 18,000 tetrahedral mesh elements were needed. Under the flow rate conditions studied, local Reynolds numbers were very low, ranging from 25 in the reactor bulk to 185 in the connecting tubes. As a result, a laminar air flow model for incompressible fluid could be used.

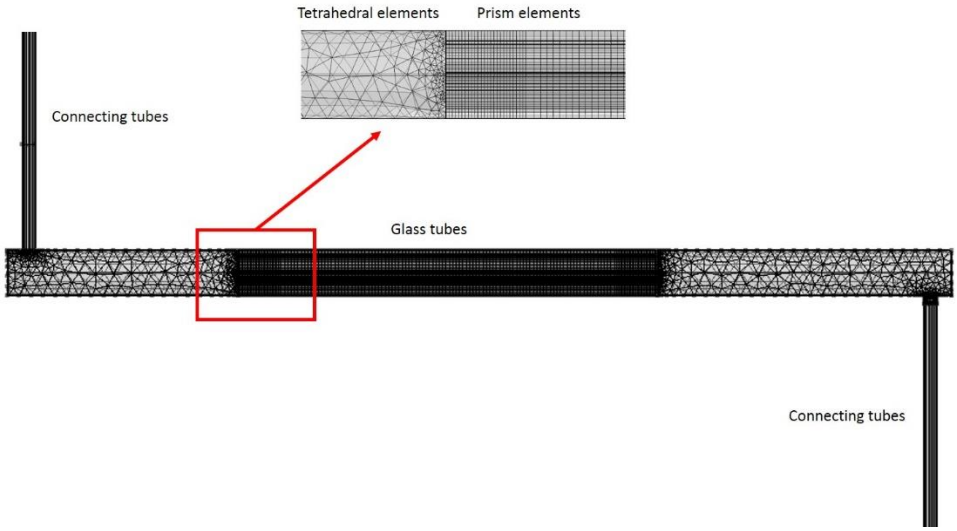

Figure 2: Representation of the mesh used in the CFD simulations.

Assuming the appropriate gas flow rate at the reactor inlet and constant atmospheric pressure at the FTIR cell outlet, a steady-state solution for the air flow velocities in the reactor was generated using a stationary solver. The transport of acetaldehyde during the transient phases

of the experiments was then modelled by coupling the time dependent advection and diffusion equation to the stationary velocity field vector **u** (Eq. 1):

$$\frac{\partial C_{Acal,bulk}}{\partial t} = \nabla \cdot \left(D \nabla C_{Acal,bulk}\right) - \mathbf{u} \cdot \nabla C_{Acal,bulk} \quad \text{(Eq. 1)}$$

With $C_{acal,bulk}$ the bulk concentration of acetaldehyde in the reactor, the FTIR cell and the tubes [mol m^{-3}], and D the mass diffusion coefficient of acetaldehyde in air [m^2 s^{-1}]. The latter value can be found in literature and was set to 1×10^{-4} m^2 s^{-1} [24]. This equation accounts for the evolution of the acetaldehyde concentration in the flow due to diffusion (first term on the right-hand side of Eq. 1) and advection (second right-hand side term) of acetaldehyde molecules.

2.3.2 Adsorption/desorption of acetaldehyde

Adsorption of pollutants on the TiO_2 surface is an essential precursory step in photocatalysis. Often Langmuir behavior is considered in which the fractional surface coverage θ_{Acal} of the adsorbed molecules is determined by the bulk concentration $C_{acal,bulk}$ and the Langmuir equilibrium constant K, defined as the ratio of the adsorption and desorption rate constants k_{ads}/k_{des} [25,26] (Eq. 2):

$$\theta_{Acal} = \frac{KC_{Acal,bulk}}{1+KC_{Acal,bulk}} = \frac{C_{Acal,ads}}{\Gamma_s} \quad \text{(Eq. 2)}$$

where $C_{AcAl,ads}$ is the surface concentration of adsorbed molecules [mol m^{-2}] and Γ_s is the maximum surface coverage, corresponding to full occupation of active sites. Simultaneous adsorption and desorption of the pollutants occur on the TiO_2 catalyst in both dark conditions and under UV illumination, and both processes should therefore be taken into account during all operation steps. Especially during transient (i.e. non-steady-state) operation of the photocatalytic reactor, knowledge of the Langmuir equilibrium constant K alone is not sufficient for accurate modelling as transitions do not occur instantaneously. In such cases, independent values for both k_{ads} and k_{des} are required to simulate the evolution of the pollutant

concentration in the system, as we will demonstrate below. In fact, whenever the pollutant concentration changes during operation, which is typical for indoor air where pollution levels may vary during the day, adsorption and desorption reactions drift away from equilibrium resulting in transient behavior. To model simultaneous adsorption and desorption, a new species $AcAl_{ads}$ with corresponding surface concentration $C_{AcAl,ads}$ was associated with the TiO_2 coated surface of the glass tubes. By doing so, we could differentiate between acetaldehyde in the bulk gas phase $AcAl_{bulk}$ and its adsorbed counterpart on the coated glass tubes $AcAl_{ads}$. Acetaldehyde adsorption was modelled as a species flux N_{ads} across the coated surface of the glass tubes [mol m^{-2} s^{-1}] from the bulk to the surface; desorption, on the other hand, was a species flux N_{des} across the same boundaries but in opposite direction (Eq. 3).

$$-\mathbf{n} \cdot \left(-D\nabla C_{Acal,bulk} + \mathbf{u} \cdot C_{Acal,bulk}\right) = -N_{ads} + N_{des} \quad \text{(Eq. 3)}$$

with **n** the normal vector pointing outward on the boundaries of the geometry. To ensure conservation of mass, the same rate expressions were used for the new species $AcAl_{ads}$; except here adsorption is a source term with positive sign and desorption is a sink term with negative sign ((Eq. 4).

$$\frac{\partial C_{Acal,ads}}{\partial t} = N_{ads} - N_{des} \quad \text{(Eq. 4)}$$

The rate expressions for acetaldehyde adsorption N_{ads} and desorption N_{des} (both in mol m^{-2} s^{-1}) on the coated surfaces are given by the typical Langmuir expressions ((Eq. 5 & (Eq. 6).

$$N_{ads} = k_{ads} C_{Acal,bulk}(1 - \theta_{Acal}) \quad \text{(Eq. 5)}$$

$$N_{des} = k_{des} \theta_{Acal} \quad \text{(Eq. 6)}$$

With k_{ads} the adsorption rate constant [m s^{-1}] and k_{des} the desorption rate constant [mol m^{-2} s^{-1}]. Only at equilibrium, the adsorption and desorption rates are equal and yield the aforementioned Langmuir expression (Eq. 2). By using separate rate expressions and appropriate rate constants

for adsorption and desorption, we were able to model transient adsorption and desorption, away from the equilibrium.

2.3.3 Photocatalytic reaction kinetics

We assumed a uniform UV intensity distribution on the coated surfaces of the glass tubes, given the small dimensions of our laboratory set-up. We also followed a straightforward approach in which the photocatalytic reaction rate is expressed by an order one with respect to the surface concentration of adsorbed molecules ((Eq. 7) [4]:

$$R_{pco} = k_{pco} C_{Acal,ads} \quad \text{(Eq. 7)}$$

where k_{pco} [s^{-1}] is the photocatalytic reaction rate constant. The photocatalytic reaction rate R_{pco} [mol m^{-2} s^{-1}] was added to the expression for the time derivative of adsorbed acetaldehyde as an extra sink term to account for the degradation of acetaldehyde on the coated surfaces of the glass tubes during illumination ((Eq. 8).

$$\frac{\partial C_{Acal,ads}}{\partial t} = N_{ads} - N_{des} - R_{pco} \quad \text{(Eq. 8)}$$

2.4 Intrinsic kinetic parameter estimation

The determination of the intrinsic kinetic parameters is based on correlating the model to the transient concentration profiles measured by FTIR, a procedure also used in our previous work [11]. In short, parameter estimation is based on fitting the experimental concentration profiles by adapting the kinetic parameters used in the models within user-defined constraints. Practically, a gradient-based Sparse Nonlinear OPTimizer (SNOPT) algorithm [27] with an optimality tolerance of 1×10^{-6} was used to find the local minimum of a least-squares objective function ((Eq. 9):

$$Obj = \sum_{t} (C_{Acal,out,exp,t} - C_{Acal,out,CFD,t})^2 \quad \text{(Eq. 9)}$$

$C_{Acal,out,exp,t}$, and $C_{Acal,out,CFD,t}$ are the experimental and predicted outlet concentrations at a particular time *t,* respectively. Both experimental and predicted concentrations are volume-averaged values for the complete FTIR detection cell, since the spectrometer uses the complete volume of the cell for measuring the absorption spectrum. The intrinsic parameters that were estimated in this study are k_{ads}, k_{des}, k_{pco} and Γ_s. By performing the experiments in different phases, as discussed earlier, we could limit the number of optimization parameters. From the results of phase (2), where adsorption equilibrium is established in dark conditions, the adsorption parameters k_{ads}, k_{des} and Γ_s were determined using the optimization solver, as no photocatalytic reaction occurred during this phase. At the start of the photocatalytic reaction phase (3), adsorption/desorption equilibrium has been established. Therefore, k_{ads}, k_{des} and Γ_s become less critical in the optimization and in principle the photocatalytic reaction rate constant k_{pco} could be determined as the only optimization parameter. An important remark is that adsorption and desorption of acetaldehyde still continue while the photocatalytic reaction is ongoing. Besides, both k_{ads} and k_{des} are not necessarily the same as in dark conditions. It has been shown that upon light excitation, the electronic band structure of TiO_2 is re-organized, which results in deviating values for the adsorption parameters as compared to those in dark conditions [28]**.** In this work, the adsorption and desorption rate constants obtained in dark conditions (phase 2) were therefore taken as initial input values in the optimization solver for fitting the acetaldehyde concentration profiles obtained for the photocatalytic reaction phase.

3. Results and discussion

3.1 FTIR spectroscopy experiments

Figure 3 shows the acetaldehyde concentration profiles monitored by the FTIR detector during the three phases of the experiment (i.e. the by-pass phase BP, the phase where adsorption-desorption equilibrium is reached under dark conditions and the illumination phase during which PCO takes place). In Figure 3, an additional adsorption phase under dark conditions was

included in order to re-establish the initial bulk acetaldehyde level. Results for three experiments with different bulk acetaldehyde concentrations are shown.

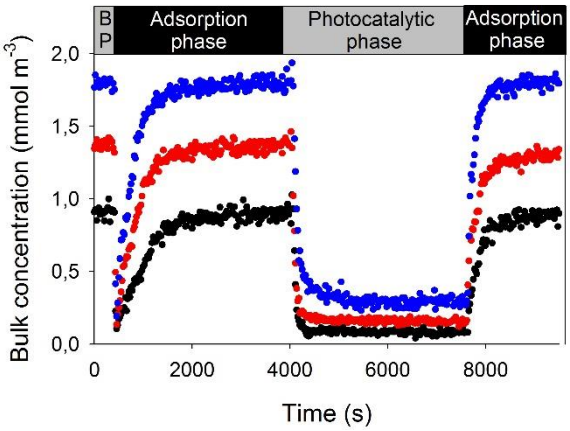

Figure 3: Transient acetaldehyde concentration profiles monitored by the FTIR detection cell.

The average acetaldehyde inlet levels, as directly derived from the steady-state concentrations in the by-pass phase, are 1.80×10^{-3}, 1.37×10^{-3} and 9.12×10^{-4} mol m^{-3} for the blue, red and black data curves respectively. In the adsorption phase, the drop in bulk acetaldehyde concentration can be explained by (1) displacement of air occupying the reactor when the valve is switched from the by-pass to the reactor and (2) adsorption of acetaldehyde on the catalytic surface. It is essential that the bulk acetaldehyde concentration returns to the same level as during the by-pass phase, as this indicates that the adsorption/desorption equilibrium is established. The adsorbed amount of acetaldehyde at equilibrium was derived by integrating the transient acetaldehyde bulk concentrations over the time period in which the rate of adsorption was greater than the rate of desorption, and subtracting the obtained value from the amount of acetaldehyde entering the reactor in the same period [20]. As in our previous work, a correction was made for the dead space in the reactor by performing the same adsorption tests with uncoated glass tubes at the same fixed flow rate and bulk acetaldehyde concentrations [11]. The as-determined amounts of adsorbed acetaldehyde in all three cases converge to a coverage

of 0.00011 mol m^{-2}, which is taken as the value for maximum surface coverage Γ_s. During the illumination phase, the photocatalytic conversion is determined to be 84%, 89% and 91% for the high, middle and low inlet concentration, respectively. Thereafter, the UV light was turned off and adsorption/desorption equilibrium is re-established.

3.2 Multiphysics Modeling

3.2.1 Air flow modelling

A typical steady-state air flow velocity profile is plotted on the symmetry plain of the geometry and shown in Figure 4. For clarity, a cross section through the glass tubes is added. The highest velocity is located in the thin connecting tubes (0.65 m s^{-1}) at the in- and outlet of the reactor. The velocity range plotted on the figure is set manually at 0 to 0.05 m s^{-1} in order to compare local differences. In the reactor tubes, typical laminar velocity profiles are observed.

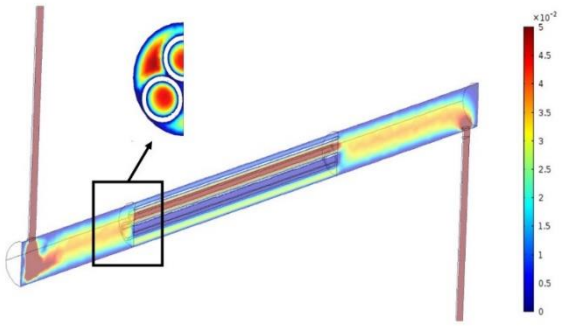

Figure 4: Modelled velocity profile in the reactor geometry under steady-state air flow (scale in m/s).

3.2.2 Kinetic parameter estimation

The experimental data obtained during the dark reactor phase are fitted with the simulated acetaldehyde bulk concentration profiles (volume-averaged values) that are obtained by applying the SNOPT algorithm. The results are shown in Figure 5.

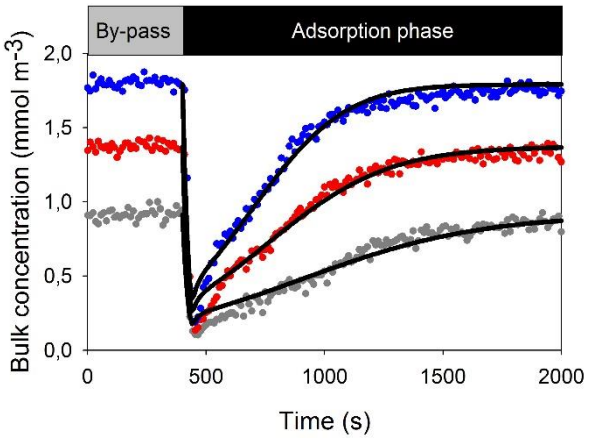

Figure 5: CFD simulations (solid lines) based on the adsorption experiments (data points) at different bulk concentrations.

The agreement of the simulations and the experimental data is good as evidenced by the overall coefficient of determination of 0.971. As initial values for the optimization routine, we used the maximum surface coverage obtained from the experiments (0.00011 mol m^{-2}) for Γ_s, and random values for k_{ads} and k_{des}. The optimized parameters k_{ads}, k_{des} and Γ_s are listed in Table 1. Notice that the experimentally determined maximum surface coverage Γ_s derived from Figure 3 is confirmed by the optimization routine. It is emphasized that for parameter estimation, the objective function ((Eq. 9) was evaluated and minimized using the complete set of experiments, i.e. the three concentration profiles for the experiments at different acetaldehyde bulk concentrations. This way, the obtained set of values for k_{ads}, k_{des} and Γ_s represent the intrinsic values that are truly independent of the acetaldehyde bulk concentration, within the concentration range of the experiments. From the obtained values of k_{ads}, k_{des} and Γ_s, the Langmuir isotherm was derived and plotted in Figure 6. It should be noticed that an experimental, analytical analysis to determine the Langmuir equilibrium constant K will fail to estimate the absolute values for k_{ads} and k_{des} independently. An important advantage of our CFD modelling approach is that by following the transient adsorption and desorption behavior, we can accurately determine independent absolute values for k_{ads} and k_{des}. This is illustrated here for one particular bulk concentration, 1.37×10^{-3} mol m^{-3} (designated by the red dotted lines in

Figure 6, a similar discussion could be conducted for the experiments at other bulk concentrations).

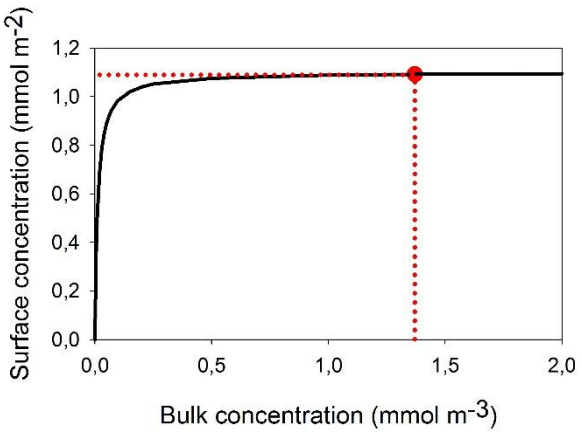

Figure 6: Langmuir adsorption isotherm obtained by the modelling optimization approach.

Figure 7a shows again the experimental transient acetaldehyde bulk concentration profile. This time, the bulk concentration profiles obtained by the model and using the optimized parameters K and Γ_s are included in the figure (curve E, black line). The other curves represent simulations for the same value of K but different absolute values for k_{ads} and k_{des} gradually varying from A to I, where A represents k_{ads} and k_{des} each divided by a factor of 10 and I represents k_{ads} and k_{des} each multiplied by a factor of 10. Figure 7b displays the transient acetaldehyde coverage on the coated surface of the glass tubes for each of these cases. As can be seen from the figures, at a particular K and Γ_s, the higher k_{ads} (and thus k_{des}), the faster the equilibrium is reached. Clearly the values of k_{ads} and $k_{des.}$ affect the shape of the concentration profile, allowing to determine them accurately using the described optimization routine.

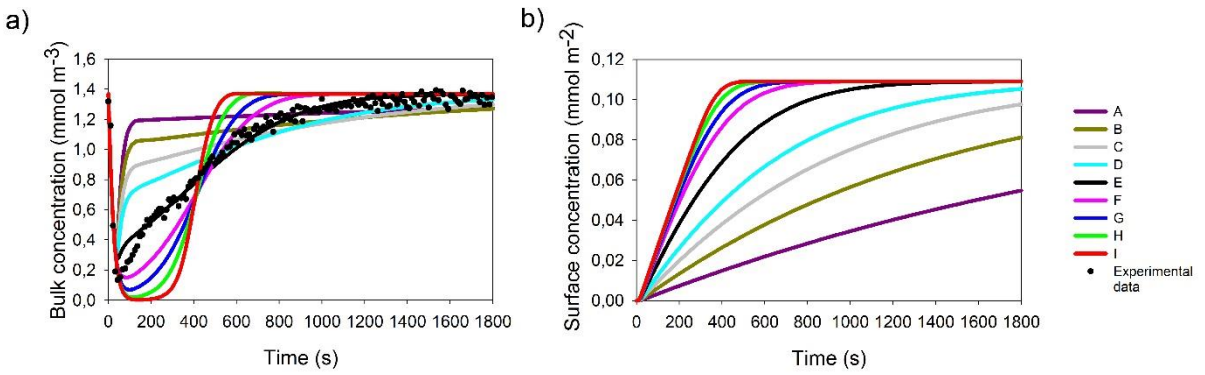

Figure 7: a) Experimental (black dots) and simulated (lines) transient acetaldehyde bulk concentration profile for the same value of K but different values of k_{ads} and k_{des} with curve E the optimized fit, A based on k_{ads} and k_{des} each divided by a factor of 10 and I based on k_{ads} and k_{des} each multiplied by a factor of 10. b) the transient acetaldehyde coverage on the coated surface of the glass tubes for those conditions.

3.2.3 Kinetic parameter estimation: adsorption/desorption and PCO in UV conditions

In a first attempt to model the transient behavior in the UV phase during which the photocatalytic reaction takes place, we used the optimization routine with a single optimization parameter, k_{pco}. In this approach, the values of k_{ads}, k_{des} and Γ_s obtained from the dark phase were used to model adsorption and desorption during the UV phase. The optimized value obtained for k_{pco} is included in Table 1.

Table 1: Optimized intrinsic kinetic parameters

Parameter	Dark phase	UV phase
$\boldsymbol{K}$ [$m^3 \cdot mol^{-1}$]	84,552	5654
$\boldsymbol{k_{ads}}$ [$m \cdot s^{-1}$]	3.295×10^{-4}	1.293×10^{-3}
$\boldsymbol{k_{des}}$ [$mol \cdot m^{-2} \cdot s^{-1}$]	3.897×10^{-9}	2.287×10^{-7}
$\boldsymbol{k_{pco}}$ [s^{-1}]	9.97×10^{-1} (a)	6.072×10^{-3}
$\boldsymbol{\Gamma_s}$ [$mol \cdot m^{-2}$]	1.101×10^{-4}	1.01×10^{-4}

(a) This is the photocatalytic reaction rate constant obtained when using k_{ads} and k_{des} from the dark adsorption phase as fixed input parameters in the optimization routine.

Despite the good agreement obtained for the adsorption phase (Figure 5), the model was not able to simulate the transient bulk acetaldehyde concentrations during the photocatalytic reaction phase using this set of kinetic parameters, as shown in Figure 8a.

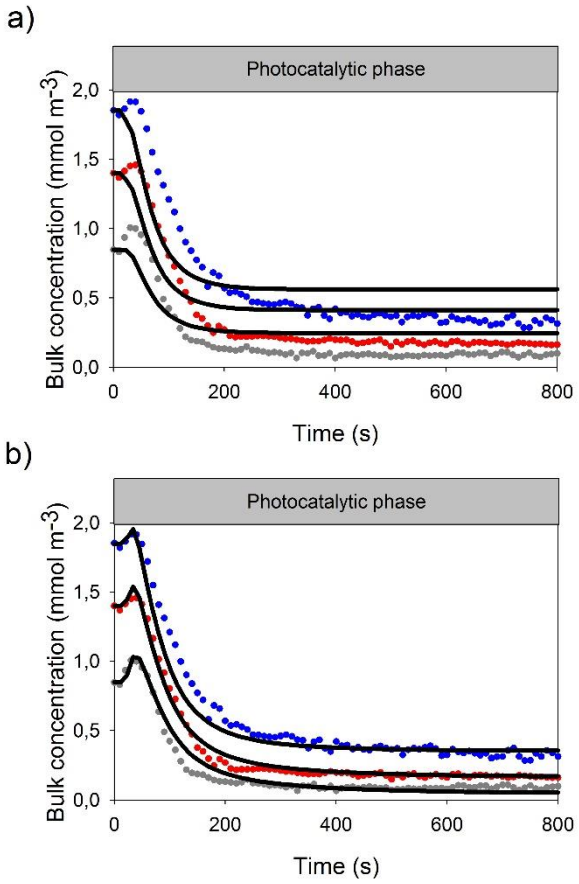

Figure 8: Optimized CFD simulations (solid lines) during the photocatalytic phase based on the experimental data at different bulk concentrations (colored data points) using the optimized kinetic parameters obtained under (a) dark conditions and (b) UV conditions.

Initially, the model underestimates the bulk acetaldehyde concentration, while the bulk concentrations at later times (when the equilibrium is reached) are clearly overestimated. To provide an explanation for the underestimation of the photocatalytic conversion by the model, the acetaldehyde coverage on the coated surface of the glass tubes, as calculated using the specific set of kinetic parameters (Table 1, 'Dark phase' column) for both the dark and the illumination phase, is shown in Figure 9a for the case of an acetaldehyde bulk concentration of 1.37×10^{-3} mol m^{-3}.

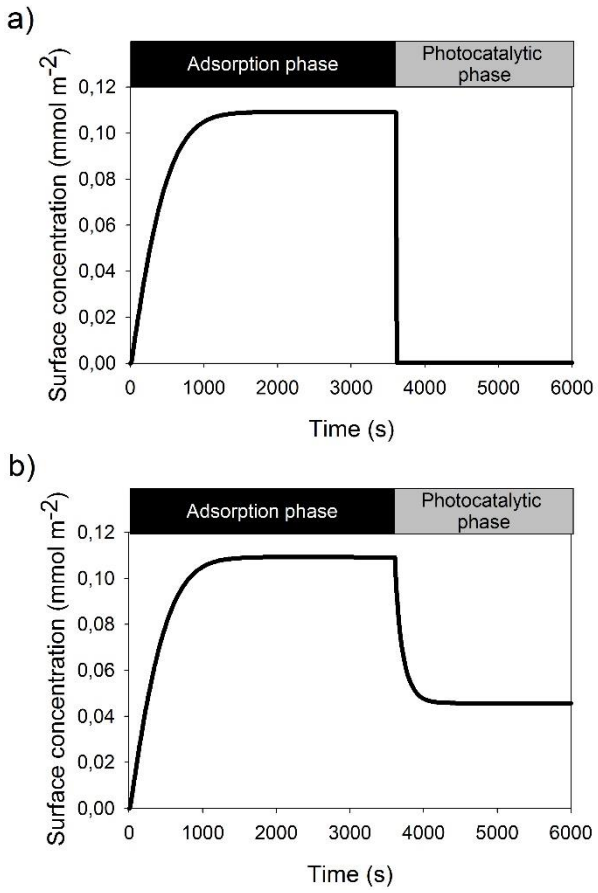

Figure 9: The transient acetaldehyde coverage on the coated surface of the glass tubes using optimized kinetic parameters under (a) dark conditions and (b) UV conditions.

As soon as the photocatalytic reaction starts, a steep drop in the concentration of adsorbed acetaldehyde is observed, indicating that the reaction is strongly limited by adsorption, at least when this set of kinetic parameters is considered. As already mentioned, k_{ads} and k_{des} are not necessarily the same in dark and UV illuminated conditions as the model results clearly confirm. When the optimization routine was used to estimate both k_{ads}, k_{des} and k_{pco} from the acetaldehyde concentration profiles corresponding to the photocatalytic reaction phase (using the adsorption and desorption rate constants obtained in dark conditions as initial guesses in the optimization routine), a new set of kinetic parameters was obtained (column 3 in Table 1). We assumed no change in Γ_s in this approach. Both k_{ads} and k_{des} have increased by at least one order of magnitude when the UV light is on. The most significant effect is observed for k_{des}, which increases by two orders of magnitude when switching on the light. As a result, the Langmuir

equilibrium constant K under UV light conditions is about 15 times smaller than the value obtained in dark conditions. When comparing the transient bulk acetaldehyde concentrations obtained for the photocatalytic reaction phase using the new set of kinetic parameters (Figure 8b), a far better agreement is observed, also evidenced by the overall coefficient of determination (0.965). Firstly, the bulk concentrations when the equilibrium is reached and the corresponding photocatalytic conversion agree well with the experiments. Secondly, the sudden 15 fold decrease of the Langmuir equilibrium constant K when the UV light is switched on, enables the model to simulate the small increase in the bulk acetaldehyde concentration at the start of the illumination phase. This sudden increase of the bulk concentration is always observed during the first 50 seconds when the UV light is switched on, although the photocatalytic reaction starts instantly after switching on the UV light. Strikingly, the optimization procedure succeeds in estimating the kinetic parameters required to simulate this behavior. For comparison, the transient acetaldehyde coverage on the coated surface of the glass tubes, as calculated using the new set of kinetic parameters (column 3 in Table 1) are plotted in Figure 9b. The reaction is no longer limited by adsorption, whereby the drop of the surface concentration when the UV light is switched on, is less pronounced, resulting in a better photocatalytic conversion.

To evaluate the validity of the final obtained intrinsic kinetic parameters, they were used to simulate the transient acetaldehyde concentration during an experiment in which the gas flow is switched directly from bypass-modus (phase 1) to reactor-illumination modus (phase 3), and this for three different initial bulk concentrations. The transient concentration profiles (Figure 10) indicate simultaneous adsorption/desorption and photocatalytic reaction, as their shape seem to be composed of a superposition of the profiles under dark and UV conditions. Obviously, we expect that in such case the intrinsic kinetic parameters under UV light condition

(column 3 in Table 1) are the best choice for the model. The corresponding CFD model results are included in Figure 10 and agree well with the experimental results.

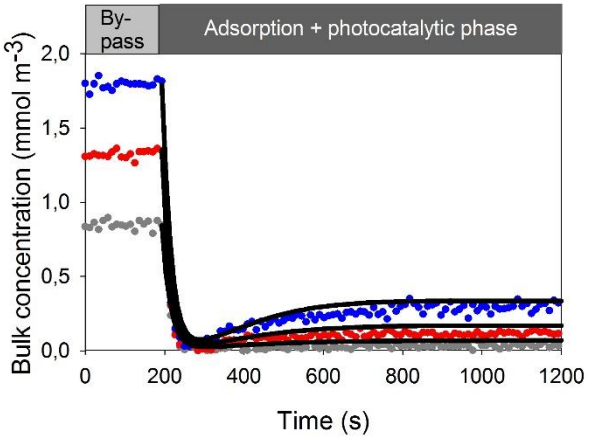

Figure 10: Validation of the CFD model by simulating the transient acetaldehyde concentration profiles for three different initial bulk concentrations sent directly through the reactor under UV illumination. Black lines: simulation, colored dots: experimental data.

From this ultimate validation test we can conclude that the intrinsic adsorption/desorption and photocatalytic reaction rate constants obtained from the modelling approach using the optimization route, are quite reliable. The obtained kinetic parameters will be very useful in further designing and upscaling of PCO air purifying units, as they can be used in CFD models for larger and more complex geometries. Equally important, the intrinsic kinetic parameters, when correctly used in a CFD model, allow evaluating the performance of PCO units in transient operating conditions.

4. Conclusions

A novel multi-tube reactor is presented that shows high photocatalytic conversion efficiencies up to 91% for an acetaldehyde concentration of ca. 1 mmol m^{-3}. Experimental data obtained from FTIR spectroscopy at the reactor outlet are used as input for a CFD model to investigate all relevant photocatalytic related parameters. Unlike analytical methods, the CFD model is able to calculate the adsorption and desorption rate constants independently, which are key

factors in determining the transient adsorption and photocatalytic behavior. The corresponding CFD simulations show excellent agreement with the experimental data with high coefficients of determination. Both adsorption and desorption rate constants are observed to increase drastically under UV conditions. The most significant effect is observed for the desorption rate constant, which increases by two orders of magnitude when switching on the lamp. This mainly affects the resulting surface concentration of acetaldehyde that in turn determines the maximal achievable photocatalytic conversion efficiency. An ultimate validation test which involves the simultaneous contributions of adsorption and photocatalysis proves that the model is a versatile and accurate tool to calculate all photocatalytic related parameters.

5. Acknowledgement

J.V.W. acknowledges the Agentschap Innoveren & Ondernemen for a PhD fellowship. S.W.V. acknowledges the Research Foundation – Flanders (FWO) for a postdoctoral fellowship.

6. References

[1] B. Kartheuser, N. Costarramone, T. Pigot, S. Lacombe, NORMACAT project: normalized closed chamber tests for evaluation of photocatalytic VOC treatment in indoor air and formaldehyde determination., Environ. Sci. Pollut. Res. Int. 19 (2012) 3763–71. doi:10.1007/s11356-012-0797-0.

[2] C.H.H. Ao, S.C.C. Lee, Indoor air purification by photocatalyst TiO2 immobilized on an activated carbon filter installed in an air cleaner, Chem. Eng. Sci. 60 (2005) 103–109. doi:10.1016/j.ces.2004.01.073.

[3] B. Sanchez, M. Sanchez-Munoz, M. Munoz-Vicente, G. Cobas, R. Portela, S. Suarez, et al., Photocatalytic elimination of indoor air biological and chemical pollution in realistic conditions, Chemosphere. 87 (2012) 625–630. doi:10.1016/j.chemosphere.2012.01.050.

[4] J. Mo, Y. Zhang, Q. Xu, J.J. Lamson, R. Zhao, Photocatalytic purification of volatile organic compounds in indoor air: A literature review, Atmos. Environ. 43 (2009) 2229–2246. doi:10.1016/j.atmosenv.2009.01.034.

[5] J. Zhao, Photocatalytic oxidation for indoor air purification: a literature review, Build. Environ. 38 (2003) 645–654. doi:10.1016/S0360-1323(02)00212-3.

[6] L. Zhong, F. Haghighat, Photocatalytic air cleaners and materials technologies – Abilities and limitations, Build. Environ. 91 (2015) 191–203. doi:10.1016/j.buildenv.2015.01.033.

[7] S.W. Verbruggen, TiO2 photocatalysis for the degradation of pollutants in gas phase: From morphological design to plasmonic enhancement, J. Photochem. Photobiol. C Photochem. Rev. 24 (2015) 64–82. doi:10.1016/j.jphotochemrev.2015.07.001.

[8] S. Verbruggen, T. Tytgat, S. Passel, J. Martens, S. Lenaerts, Cost-effectiveness analysis to assess commercial TiO2 photocatalysts for acetaldehyde degradation in air, Chem. Pap. 68 (2014) 1273–1278. doi:10.2478/s11696-014-0557-3.

[9] M. Sleiman, P. Conchon, C. Ferronato, J.-M. Chovelon, Photocatalytic oxidation of toluene at indoor air levels (ppbv): Towards a better assessment of conversion, reaction intermediates and mineralization, Appl. Catal. B Environ. 86 (2009) 159–165. doi:10.1016/j.apcatb.2008.08.003.

[10] G.B. Raupp, A. Alexiadis, M.M. Hossain, R. Changrani, First-principles modeling, scaling laws and design of structured photocatalytic oxidation reactors for air purification, Catal. Today. 69 (2001) 41–49. doi:10.1016/S0920-5861(01)00353-4.

[11] S.W. Verbruggen, M. Keulemans, J. van Walsem, T. Tytgat, S. Lenaerts, S. Denys, CFD modeling of transient adsorption/desorption behavior in a gas phase photocatalytic fiber reactor, Chem. Eng. J. 292 (2016) 42–50. doi:10.1016/j.cej.2016.02.014.

[12] D.B. Warheit, T.R. Webb, K.L. Reed, S. Frerichs, C.M. Sayes, Pulmonary toxicity study in rats with three forms of ultrafine-TiO2 particles: Differential responses related to surface properties, Toxicology. 230 (2007) 90–104. doi:10.1016/j.tox.2006.11.002.

[13] S.J. Klaine, P.J.J. Alvarez, G.E. Batley, T.F. Fernandes, R.D. Handy, D.Y. Lyon, et al., Nanomaterials in the environment: behavior, fate, bioavailability, and effects., Environ. Toxicol. Chem. 27 (2008) 1825–1851. doi:10.1897/08-090.1.

[14] J. Zhang, W. Song, J. Guo, J. Zhang, Z. Sun, L. Li, et al., Cytotoxicity of different sized TiO2 nanoparticles in mouse macrophages, Toxicol. Ind. Health. 29 (2012) 523–533. doi:10.1177/0748233712442708.

[15] S.W. Verbruggen, S. Lenaerts, S. Denys, Analytic versus CFD approach for kinetic modeling of gas phase photocatalysis, Chem. Eng. J. 262 (2015) 1–8. http://linkinghub.elsevier.com/retrieve/pii/S1385894714012273 (accessed April 4, 2016).

[16] S. Brosillon, L. Lhomme, C. Vallet, A. Bouzaza, D. Wolbert, Gas phase photocatalysis and liquid phase photocatalysis: Interdependence and influence of substrate concentration and photon flow on degradation reaction kinetics, Appl. Catal. B Environ. 78 (2008) 232–241. doi:10.1016/j.apcatb.2007.09.011.

[17] I. Di Somma, L. Clarizia, S. Satyro, D. Spasiano, R. Marotta, R. Andreozzi, A kinetic study of the simultaneous removal of EDDS and cupric ions from acidic aqueous solutions by TiO2-based photocatalysis under artificial solar light irradiation and deaerated batch conditions, Chem. Eng. J. 270 (2015) 519–527. doi:10.1016/j.cej.2015.01.056.

[18] R. Dillert, J. Stotzner, A. Engel, D.W. Bahnemann, Influence of inlet concentration and light intensity on the photocatalytic oxidation of nitrogen(II) oxide at the surface of Aeroxide TiO2 P25, J. Hazard. Mater. 211-212 (2012) 240–246. doi:10.1016/j.jhazmat.2011.11.041.

[19] Y. Chen, D.D. Dionysiou, TiO2 photocatalytic films on stainless steel: The role of Degussa P-25 in modified sol-gel methods, Appl. Catal. B Environ. 62 (2006) 255–264. doi:10.1016/j.apcatb.2005.07.017.

[20] S.W. Verbruggen, K. Masschaele, E. Moortgat, T.E. Korany, B. Hauchecorne, J.A. Martens, et al., Factors driving the activity of commercial titanium dioxide powders towards gas phase photocatalytic oxidation of acetaldehyde, Catal. Sci. Technol. 2 (2012) 2311–2318. doi:doi: 10.1039/C2CY20123B.

[21] B. Hauchecorne, D. Terrens, S. Verbruggen, J.A. Martens, H. Van Langenhove, K. Demeestere, et al., Elucidating the photocatalytic degradation pathway of acetaldehyde: An FTIR in situ study under atmospheric conditions, Appl. Catal. B Environ. 106 (2011) 630–638. doi:10.1016/j.apcatb.2011.06.026.

[22] S.W. Verbruggen, S. Deng, M. Kurttepeli, D.J. Cott, P.M. Vereecken, S. Bals, et al., Photocatalytic acetaldehyde oxidation in air using spacious TiO2 films prepared by atomic layer deposition on supported carbonaceous sacrificial templates, Appl. Catal. B Environ. 160-161 (2014) 204–210. doi:10.1016/j.apcatb.2014.05.029.

[23] S. Deng, S.W. Verbruggen, Z. He, D.J. Cott, P.M. Vereecken, J. a. Martens, et al., Atomic layer deposition-based synthesis of photoactive TiO2 nanoparticle chains by using carbon nanotubes as sacrificial templates, RSC Adv. 4 (2014) 11648. doi:10.1039/c3ra42928h.

[24] R.L. Sherwood, C.R., Pigford, T. K., Wilke, Mass Transfer, McGraw-Hill, New York, 1965.

[25] M.L. Sauer, D.F. Ollis, Photocatalyzed Oxidation of Ethanol and Acetaldehyde in Humidified Air, J. Catal. 158 (1996) 570–582. doi:10.1006/jcat.1996.0055.

[26] A. V. Vorontsov, V.P. Dubovitskaya, Selectivity of photocatalytic oxidation of gaseous ethanol over pure and modified TiO2, J. Catal. 221 (2004) 102–109. doi:10.1016/j.jcat.2003.09.011.

[27] P.E. Gill, W. Murray, M.A. Saunders, SNOPT: An SQP Algorithm for Large-Scale Constrained Optimization, SIAM J. Optim. 12 (2002) 979–1006. doi:10.1137/S1052623499350013.

[28] Y. Xu, C.H. Langford, Variation of Langmuir adsorption constant determined for TiO2-photocatalyzed degradation of acetophenone under different light intensity, J. Photochem. Photobiol. A Chem. 133 (2000) 67–71. doi:10.1016/S1010-6030(00)00220-3.

Figure 1: CFD geometry including the test reactor, connecting tubes and FTIR detection cell.

Figure 2: Representation of the mesh used in the CFD simulations.

Figure 3: Transient acetaldehyde concentration profiles monitored by the FTIR detection cell.

Figure 4: Modelled velocity profile in the reactor geometry under steady-state air flow (scale in m/s).

Figure 5: CFD simulations (solid lines) based on the adsorption experiments (data points) at different bulk concentrations.

Figure 6: Langmuir adsorption isotherm obtained by the modelling optimization approach.

Figure 7: a) Experimental (black dots) and simulated (lines) transient acetaldehyde bulk concentration profile for the same value of K but different values of kads and kdes with curve E the optimized fit, A based on kads and kdes each divided by a factor of 10 and I based on kads and kdes each multiplied by a factor of 10. b) the transient acetaldehyde coverage on the coated surface of the glass tubes for those conditions.

Figure 8: Optimized CFD simulations (solid lines) during the photocatalytic phase based on the experimental data at different bulk concentrations (colored data points) using the optimized kinetic parameters obtained under (a) dark conditions and (b) UV conditions.

Figure 9: The transient acetaldehyde coverage on the coated surface of the glass tubes using optimized kinetic parameters under (a) dark conditions and (b) UV conditions.

Figure 10: Validation of the CFD model by simulating the transient acetaldehyde concentration profiles for three different initial bulk concentrations sent directly through the reactor under UV illumination. Black lines: simulation, colored dots: experimental data.